Available online at www.sciencedirect.com
SCIENCE DIRECT
Polymer 47 (2006) 2894–2903
polymer
www.elsevier.com/locate/polymer

Analysis of phase morphology and dynamics of immiscible PP/PA1010 blends and its partial-miscible blends during melt mixing from SEM patterns

Li-Tang Yan [a,b], Jing Sheng [b,*]

[a] Advanced Materials Laboratory, Department of Chemical Engineering, Tsinghua University, Beijing 100084, People's Republic of China
[b] School of Material Science and Engineering, Tianjin University, Tianjin 300072, People's Republic of China

Received 23 September 2004; received in revised form 24 December 2005; accepted 19 February 2006
Available online 10 March 2006

Abstract

The formation and evolution of the phase morphology of polypropylene (PP) with Nylon1010 (PA1010) blends before and after adding the compatibilizer, polypropylene grafted maleic anhydride (PP-*g*-MAH), during melt mixing are investigated by the pattern analysis of scanning electron microscope (SEM). The average particle diameter DP_{AV}, characteristic length Λ and the average characteristic length Λm are calculated to discuss the melt mixing process. It is proved, by the figure-estimation theory, that the distribution of Λ is log–normal distribution. Furthermore, the phase morphology during melt mixing is discussed in depth by the parameters of the log–normal distribution. The results demonstrate that the structure of the dispersed phase during melt mixing evolves with dynamical self-similarity through the competition of break-up and coalescence of dispersed phase. A fractal dimension, based on the probability density of the character length, is calculated in this study. The results show that the fractal dimension is an effective parameter to characterize the melt mixing process of polymer blends.

Keywords: Polymer blends; Character length; Fractal

1. Introduction

Polymer blending offers an extraordinary rich range of new materials with enhanced characteristics regarding optical, chemical or mechanical performance [1,2]. Correspondingly, the study on binary polymer blends has been significantly increasing during past few years due to the important implications in both science and technology [3–6]. The performance of the polymer material can be efficiently improved by combining existing polymers with suitable way. It is realized that the properties of polymer blends, including strength, toughness, etc. have tight relations with their internal microscopic phase morphology [7–9]. Moreover, the formation and evolution of the phase morphology strongly depends on the melt mixing process. Thus, the dynamics during melt mixing has a large effect on the macroscopic properties of the blends, and has also been reported in many works [10–15].

The microscopic phase morphology of polymer alloys can be directly observed by some microscopy methods, e.g. SEM, TEM (transmission electron micrograph), etc. The patterns of SEM indicate the information of some physical parameters, such as component concentration and orientation, in the space. As a matter of fact, the pattern formation and selection are equivalent to the formation and controlling of the phase morphology in polymer material science [16]. If assisted by digital image analysis, the formation mechanism and evolution dynamics of the phase morphology can be qualitatively or quantitatively studied. For example, Corté and his coworkers [9] presented a simple method based on image analysis of TEM to estimate both distributions in particle size and ligament thickness, recently. However, the report about the study on the dynamics of the phase morphology during melt mixing through patterns is rare. On the other hand, after the scaling theory was introduced into polymer field, the understanding of the polymer systems has been much extended [17–20]. In fact, the scaling behavior of some physical phenomena corresponds to the self-similarity in the space or time. Thus, these physical phenomena may have some relations with the fractal behavior [22–24]. However, the potential fractal behavior in the phase formation and

* Corresponding author. Tel.: +86 22 274 06647.
E-mail address: shengxu@public.tpt.tj.cn (J. Sheng).

0032-3861/$ - see front matter © 2006 Elsevier Ltd. All rights reserved.
doi:10.1016/j.polymer.2006.02.048

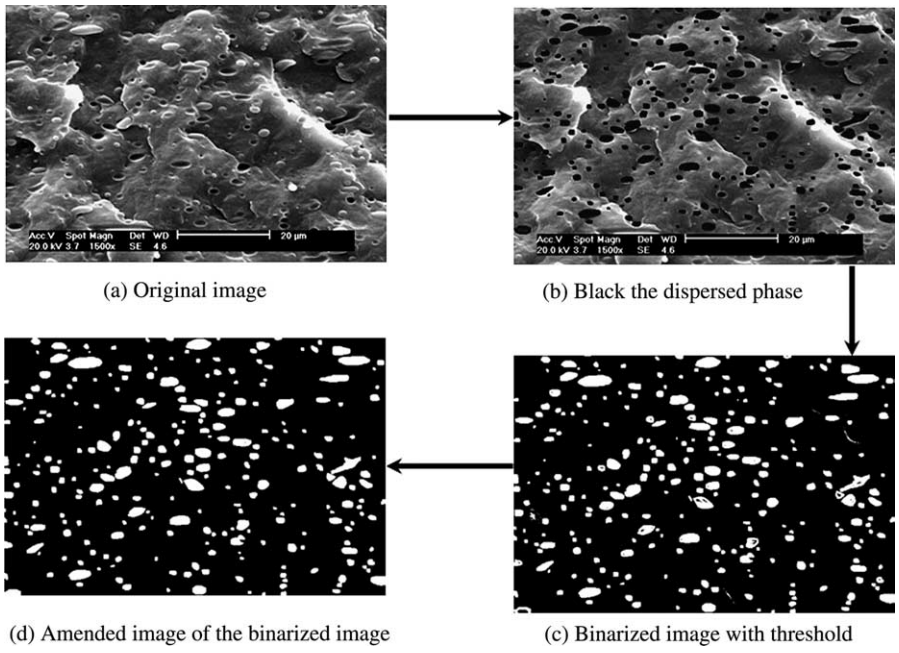

Fig. 1. The binarizing process of the image of PP/PA1010 blends (90/10) at 1 min.

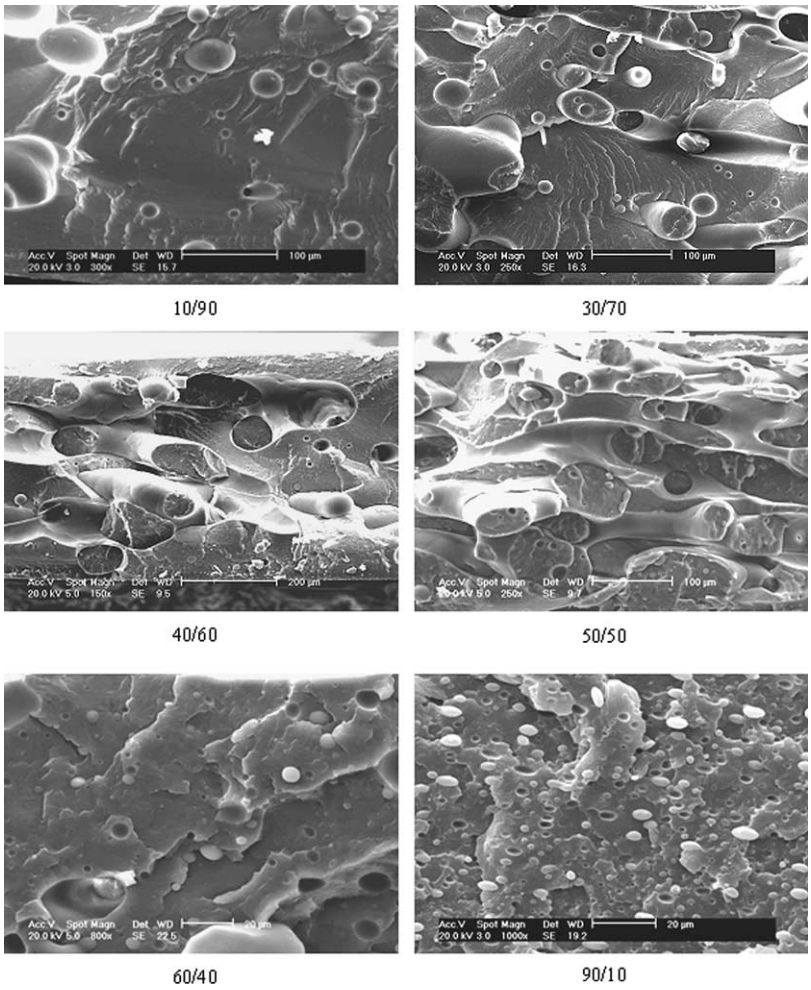

Fig. 2. SEM patterns of PP/PA1010 immiscible blends with different factions.

evolution dynamics of polymer blends have been paid rare attention up to now.

In the present paper, based on the image analysis of SEM patterns, the phase formation and evolution dynamics of the PP/PA1010 systems, before and after adding the compatibilizer (PP-*g*-MAH), are investigated. The average particle size and the distribution in particle size are discussed in detail. Furthermore, the fractal theory was used to explore the phase evolution dynamics in this melt mixing process in depth.

2. Experimental

2.1. Experimental materials

The PP in this study was a commercial polymer from Beijing Yanshan Petrifaction Co. (China) with $\rho = 0.90$ g/cm^3 and $T_m = 164$–167 °C. The PA1010 was a commercial polymer from Tianjin Zhonghe Chemical Plant (China) with $\rho = 1.03$–1.05 g/cm^3 and $T_m = 198$–210 °C. PP-*g*-MAH was also a commercial polymer from Yueyang Changling Chemical Plant (China) with percentage of grafting 2.5.

2.2. Blends preparation

An XSM-1/20-80 rubber mixer with total volume 50 cm^3 was used to prepare the blends. The mixer runs for all systems were done at 32 rpm. PP/PA1010/PP-*g*-MAH (90/10/5,80/20/5,70/30/5, 60/40/5,50/50/5,40/60/5,30/70/5,20/80/5, 10/90/5) were washed by distilled water, respectively. It should be noted that the volume fraction is used for all the compositions in this study. The pellets were dry before being fed into the mixer. The feeding began at 0 s, and was completed in approximately 30 s. The temperature of the mixer wall was controlled at about 220 °C and the total mixing time was 13 min. Some samples were taken at different times (PP/PA1010/ PP-*g*-MAH = 90/10/5; 1, 2, 3, 4, 5, 7, 9, 12 min). Others were taken at 12 min. The samples should be put into the ice water quickly. PP/PA1010 samples were prepared with the same method.

2.3. Microscopy

The samples were cooled in liquid nitrogen for 10 min, then, were fractured quickly. The Au–Pd was sprayed on the phase

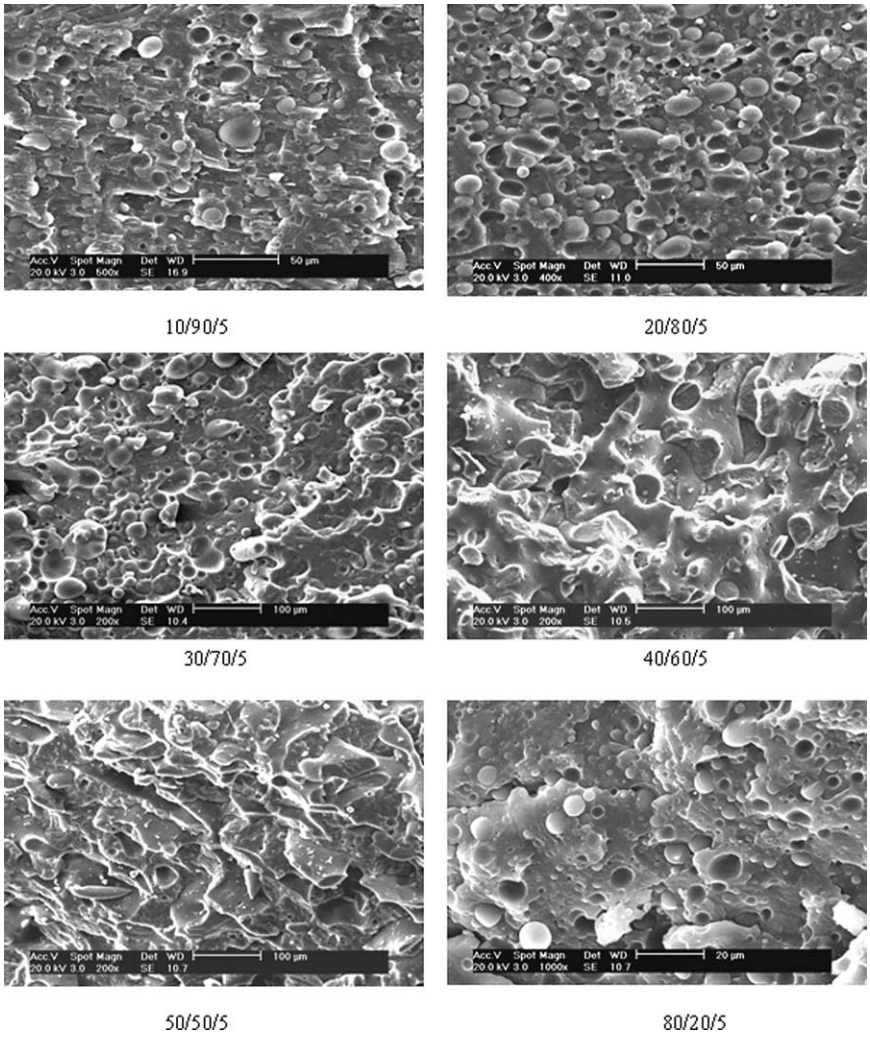

Fig. 3. SEM patterns of PP/PA1010/PP-*g*-MAH partial-miscible blends with different fractions.

surface. A scanning electron scope (Philips XL-30) was used to observe the phase morphology of the samples.

2.4. Data collection

All results about the particle size and the character length were obtained by a digital image process software (EMPP) edited by our group. The software only treats binarized images: white particles for instance, distributed in black matrix. Such images can be difficult to obtain because accurate binarization requires a clear initial image with good contrast between matrix and particles. Here, we only focus on the data treatment once the image has been binarized. As an example, a detailed binarizing process used in the work is presented in Fig. 1.

Using the image analysis software, one can collect much information for each particle such as its cross-sectional area, character chain length, etc. An area equivalent diameter, DP_{AV}, is defined for each particle as the diameter for a circle of the same cross-sectional area. It is given by

$$DP_{AV} = 2\sqrt{\frac{A}{\pi}} \tag{1}$$

where A is the cross-sectional area of the particle measured on the micrograph.

The spatial brightness distribution of the binarized images can be measured by scanning them along different degrees and with different scanning densities by this software. The repeated distance and its histogram thus measured were identical in the different directions and reflect histogram of a characteristic length, Λ, for the phase-dispersing morphology [21]. The probability density $P(\Lambda)$ can be defined by finding Λ from a frequency of the events $N(\Lambda)$,

$$P(\Lambda) = \frac{N(\Lambda)}{\int_0^{+\infty} N(\Lambda)\mathrm{d}\Lambda} \tag{2}$$

A normalized probability function $P(\Lambda/\Lambda m)$ is further defined by

$$P(\Lambda/\Lambda m) \equiv P(\Lambda)\Lambda m/c \tag{3}$$

in order to compare the shapes of the probability density distribution functions $P(\Lambda)$ obtained at different mixing times. Here, Λm is the average characteristic length defined by

$$\Lambda m = \int_0^{+\infty} \Lambda P(\Lambda)\mathrm{d}\Lambda \tag{4}$$

$P(\Lambda/\Lambda m)$ is dimensionless, and the constant c is defined by

$$\int_0^{+\infty} P(\Lambda/\Lambda m)\mathrm{d}(\Lambda/\Lambda m) = 1/c \tag{5}$$

Furthermore, by plotting $P(\Lambda/\Lambda m)$ against the normalized characteristic length $\Lambda/\Lambda m$, the shapes of $P(\Lambda/\Lambda m)$ obtained at different times can be compared. Thus, the function of $P(\Lambda/\Lambda m)$ can be used as a scaling function to study the self-similarity of the phase morphology during melt mixing.

3. Results and discussion

3.1. Evolution of the phase morphology during melt mixing

The typical morphologies of the PP/PA1010 blends with different fractions, before and after adding the compatibilizer, are shown in Figs. 2 and 3. It can be found that, when the fractions of PP/PA1010/PP-*g*-MAH are from 90/10/5 to 70/30/5, PA1010 particles dispersed within the PP matrix. The 60/40/5 and 50/50/5 blends show somewhat interconnected morphologies. Comparing these two figures, one can observe that the phase inversion takes place when PP, instead of PA1010, is the major component after adding the compatibilizer. There are many big cells of the dispersed phase in the images when PP is the minor component. Fig. 4(a) and (b) plots the average size, Λm and DP_{AV}, of the dispersed phase against the component fraction and the mixing time, respectively. It can be seen from Fig. 4(a) that the adding of the compatibilizer causes a further decrease in particle size. Fig. 4(a) also shows that, after adding the compatibilizer, the

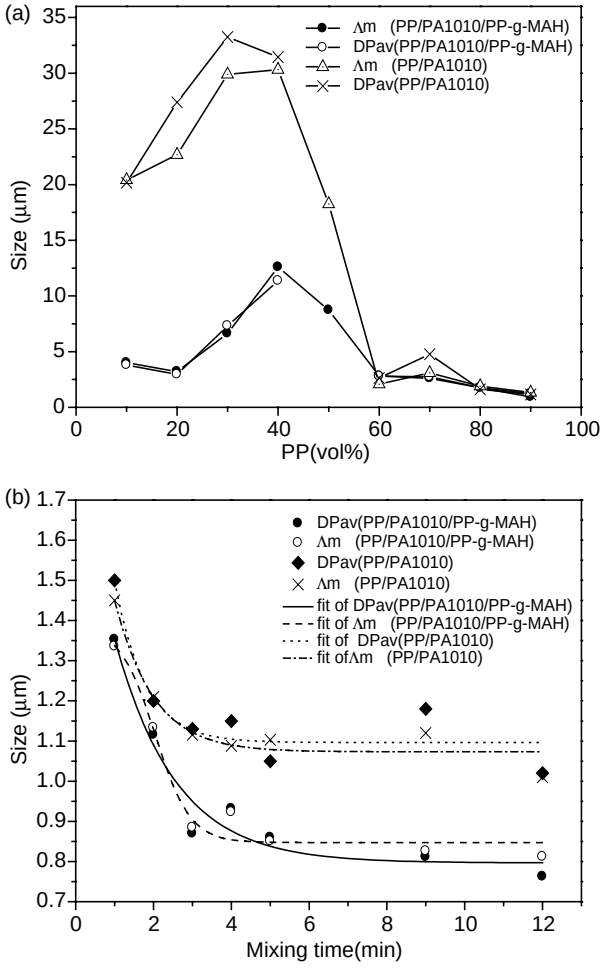

Fig. 4. SEM patterns of PP/PA1010/PP-*g*-MAH (90/10/5) partial-miscible blends during melt mixing.

dispersed phase diameter changes more sharply when PP is the dispersed phase, which demonstrates that PA1010 is easier to disperse. All above analysis proves a fact that the compatibilizer can retard the coalescence of dispersed phase, especially when PP, which vicious is smaller during melt mixing, is dispersed phase, corresponding to the report of Han C D et al. [25].

Figs. 5 and 6 are SEM patterns of PP/PA1010 (90/10) at different times before and after adding the compatibilizer. Fig. 4(b) indicates the variations of the average size of the dispersed phase particles with mixing time. It can be seen that the particles become smaller and their shapes become uniform with the mixing time. Fig. 4(b) shows that the average sizes of the dispersed phase particles decrease more sharply in the stage before 2 min. According to the report of Elemans et al. [26], this is the initial stage of the mixing when the dispersed phase breaks up. After 2 min the sizes of the particles are almost unchangeable although their shapes approximate to circle due to the coalescence of the smaller dispersed phase particles. The break-up and coalescence of the dispersed phase particles come to balance gradually at the medium and later stages. Thus, the morphology of the dispersed phase is almost unchangeable after 2 min. These results imply that the phase morphology mainly forms at the initial stage, i.e. 0–2 min after beginning of the melt mixing. Fig. 4(b) also reflects that Λm and DP_{AV} become smaller after adding the compatibilizer, demonstrating that the compatibilizer can retard the coalescence of dispersed phase.

Fig. 4 also shows that the changes of Λm are in a good agreement with those of DP_{AV}. Both the variation trends and the values of these two parameters are very similar, demonstrating that Λ and Λm can be used to characterize the size and size distribution of the dispersed phase. They should also be effective parameters to characterize the dynamics of the phase dispersion during melt mixing. Moreover, it is worth note that Λ and Λm can be used to analysis the phase structure with the interconnected morphology which is difficult to be deal with by the average particle diameter.

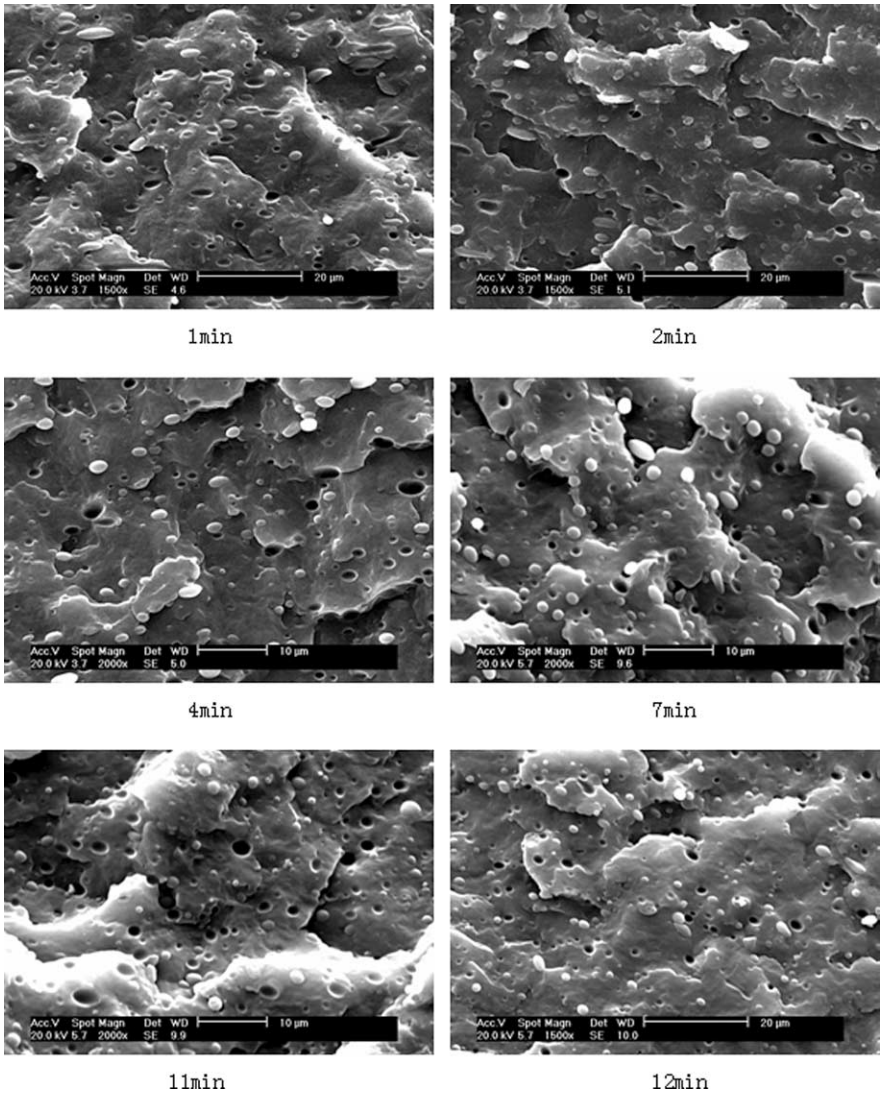

Fig. 5. Plots of Λm, DP_{AV} against the composition fraction and the melt mixing time. (A) The composition fraction. (B) The melt mixing time (90/10).

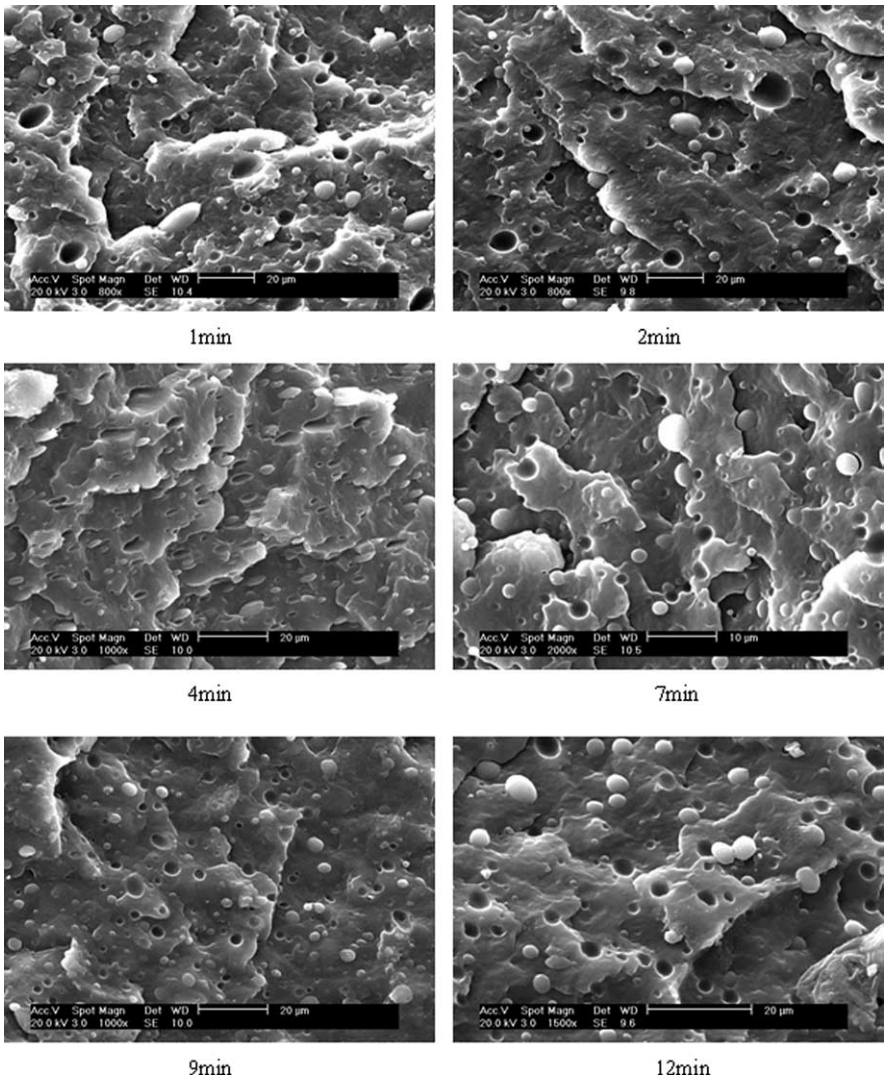

Fig. 6. SEM patterns of PP/PA1010 (90/10) immiscible blends during melt mixing.

3.2. Distribution in average particle size

For many particle dispersions [27] and for polymer blends in particular [28], the distribution in particle size often obeys a log–normal distribution. Such statistical law is given by the following density, $F(t)$

$$F(t) = \frac{\lg e}{\sqrt{2\pi}\sigma t} \int_{-\infty}^{t} \exp\left[-\frac{1}{2}\left(\frac{\lg t - \mu}{\sigma}\right)^2\right] \mathrm{d}t \tag{6}$$

for $t \in [0, +\infty]$

where σ and μ are the standard deviation and number average of the distribution in $\ln(t)$, respectively. Here, the figure-estimation theory is introduced to judge whether the distributions of the systems concerned in the present study are the log–normal distribution [29]. Detailed calculations leading to the figure-estimation theory are given in the Appendix A. It can be found that, in terms of this theory, Eq. (6) can be transformed into the following form in the $X-Y$ coordinate system

$$Y = \frac{1}{\sigma}X - \frac{\mu}{\sigma} \tag{7}$$

where X and Y are the parameters in the $X-Y$ coordinate system.

Fig. 7 is the $P(\Lambda)-\Lambda$ histogram of PP/PA1010 (90/10) blends at 1 min during melt mixing, which is randomly selected from all the systems. The histogram shows that the distribution of Λ is similar to the log–normal distribution. According to the figure-estimation theory, a log–normal distribution function corresponds to an ascending line in the $X-Y$ coordinate system. On the other hand, an ascending line in the $X-Y$ coordinate system will ascertain a log normal distribution function. Thus, one can use the one by one relation to determine whether the distribution function of Λ is log normal

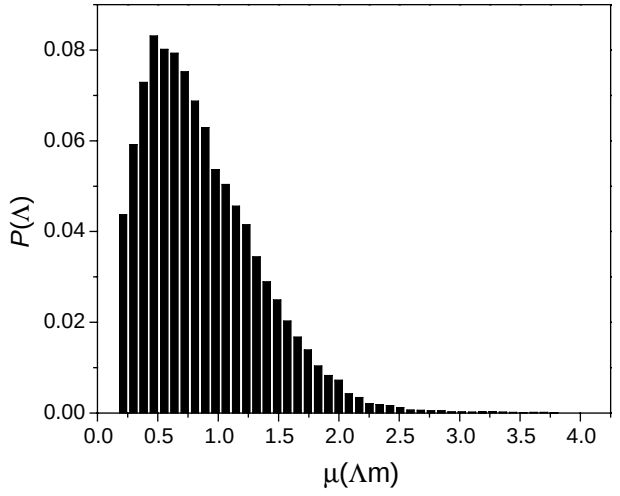

Fig. 7. $P(\Lambda)-\Lambda$ histogram of PP/PA1010 blends at 1 min during melt mixing.

distribution. Fig. 8(a) and (b) shows that the distributions of Λ, with different fractions and at different times, can be transformed into ascending lines. So the distribution of Λ is log–normal distribution.

Based on Eq. (7), the σ and μ in the distribution function of Λ can be obtained by linear regression. σ and e^{μ} characterize the range of the distribution and the utmost size of the

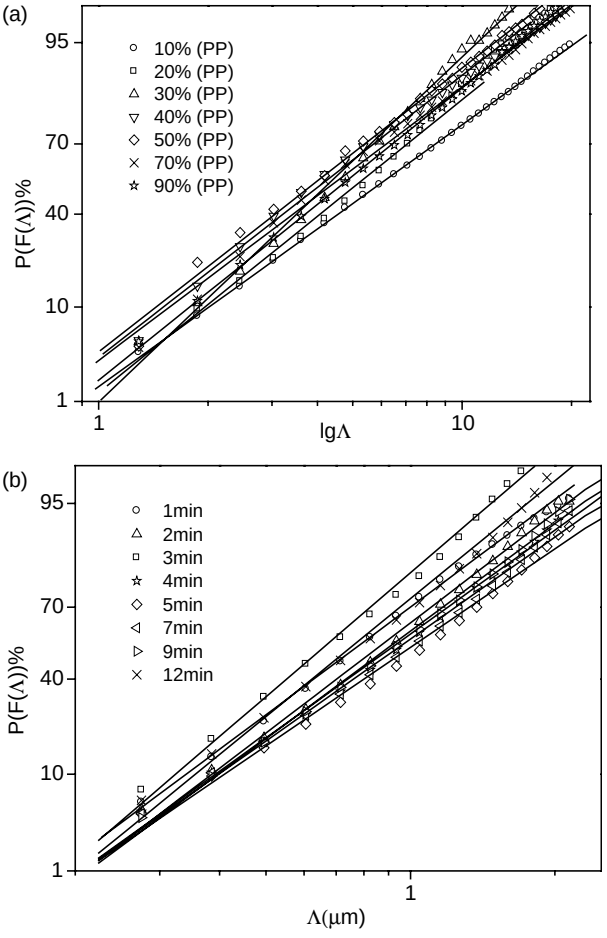

Fig. 8. Plots of $P(F(\Lambda))\%$ against Λ for PP/PA1010 blends. (a) The composition fraction. (b) The melting time (90/10).

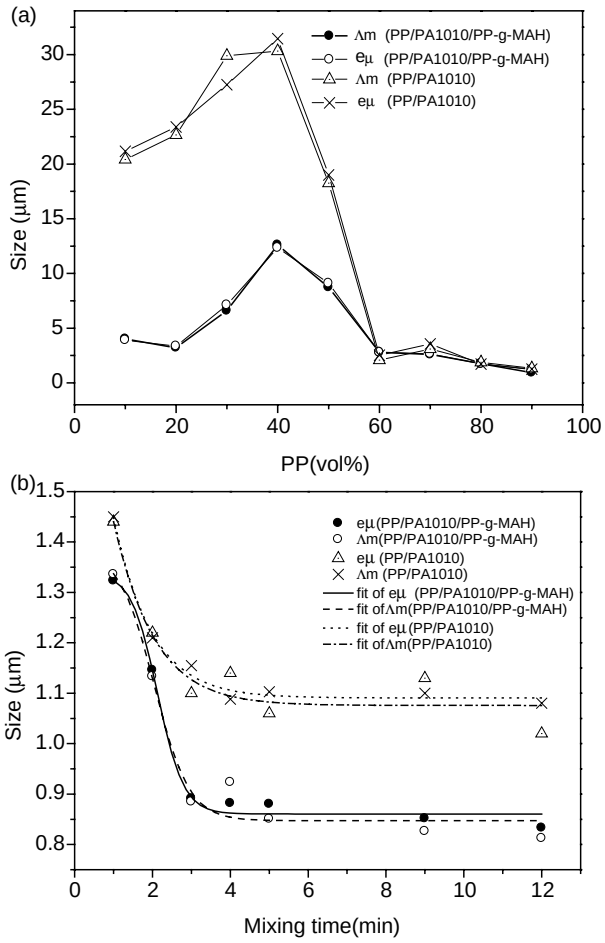

Fig. 9. Plots of Λm, e^{μ} against the composition fraction and the melt mixing time. (a) The composition fraction. (b) The melt mixing time (90/10).

dispersed phase particle diameters respectively. Fig. 9(a) and (b) indicates that the changes of e^{μ} are almost the same as those of Λm. Fig. 10(a) shows that, with the increasing fraction of the dispersed phase, the distribution range of Λ become wider, and the distribution range comes to the widest near the phase inversion. Fig. 10(b) shows that the distribution range of Λ becomes narrower during melt mixing. Furthermore, it can be found from both Figs. 9 and 10 that the distribution range of the dispersed phase particle becomes narrower after feeding the compatibilizer. All above analysis implies that σ and e^{μ} are two effective parameters to characterize the dynamics of phase dispersion during melt mixing.

3.3. Fractal behavior analysis of the SEM patterns during melt mixing

We would like to discuss the fractal behavior of the patterns in this region. Whether the distribution of Λ has the self-similar region, i.e. the dimensionless region, or not should be judged first. The dimensionless is that some characters, e.g. the normalized shape, of the fractal object do not change with the variation of scale [22–24]. Secondly, the range of the dimensionless region should be determined because only in the

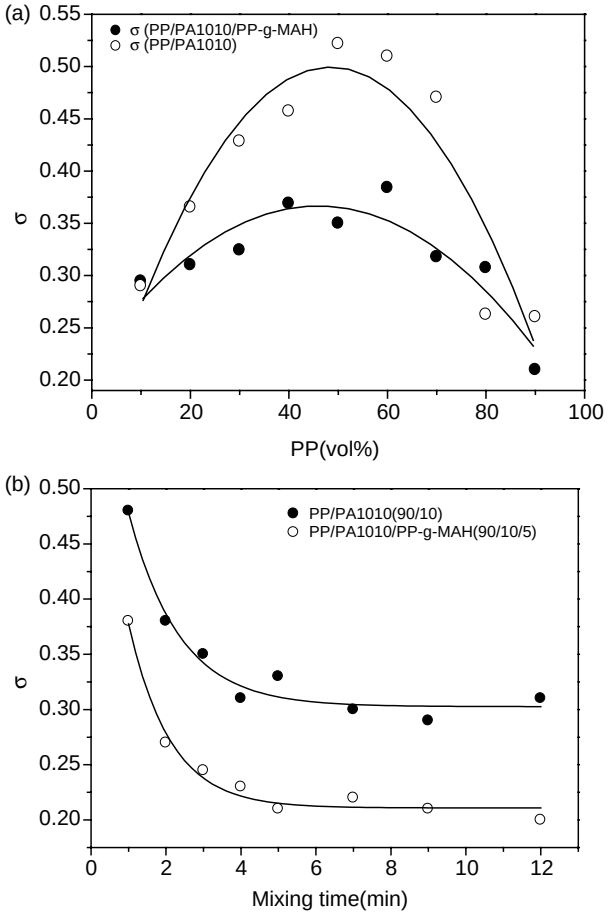

Fig. 10. Plots of σ against the composition fraction and the melt mixing time. (a) The composition fraction. (b) The melt mixing time (90/10).

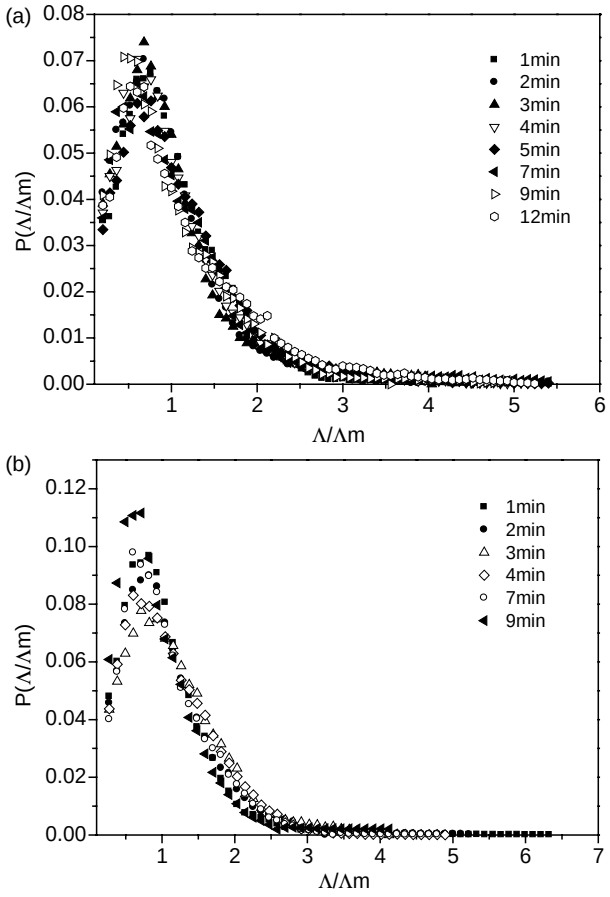

Fig. 11. Plots of $P(\Lambda/\Lambda m)$ against $\Lambda/\Lambda m$for PP/PA1010 and PP/PA1010/PP-*g*-MAH blends. (a) PP/PA1010 (90/10). (b) PP/PA1010/PP-*g*-MAH (90/10/5).

dimensionless region the fractal dimension can be calculated by the linear regression [22–24]. As stated earlier, the function of $P(\Lambda/\Lambda m)$ can be used as a scaling function to study the self-similarity of the phase morphology during melt mixing by comparing the histograms of $P(\Lambda/\Lambda m)$ at different times.

Fig. 11 shows the plots of $P(\Lambda/\Lambda m)$ against $\Lambda/\Lambda m$, with the composition fractions PP/PA1010/PP-*g*-MAH (90/10/5) and PP/PA1010 (90/10), at different times during melt mixing. The figure reflects that the curves, obtained at different times in the medium and later stages of melt mixing, fall on a master curve. This demonstrating that PP/PA1010 blend systems, before and after adding the compatibilizer, are self-similar at the time, especially in the medium and later stages during melt mixing. Thus we obtained the following conclusion: The structure of the dispersed phase during melt mixing evolves with dynamical self-similarity through the competition of break-up and coalescence of dispersed phase.

Furthermore, the fractal dimension can be calculated after determining the self-similarity of the phase morphologies at different times. The fractal dimension, D, calculated from the probability density of Λ, $P(\Lambda)$, is given by the following expression:

$$\lg P(\Lambda) \propto (-D-1)\lg \Lambda \tag{8}$$

Detailed deduction leading to Eq. (8) is given in the Appendix B. The fractal dimension D corresponds to other fractal dimensions defined by coarse-graining, and can characterize the surface fractal [23]. When the dispersed phase completely fills the pattern, D is 2, otherwise, D is between 1 and 2. D becomes bigger with the increasing density of the dispersed phase. For a certain composition fraction, D is bigger if the dispersion degree of the dispersed phase is higher.

Fig. 12 is the plot of $\lg P(\Lambda)$ versus $\lg \Lambda$ at 4 min during melt mixing. The pattern is randomly selected from all patterns. The figure shows that there is a dimensionless region when $\lg \Lambda$ is from 0.21 to 0.72. Why the dimensionless region is only from 0.21 to 0.72? In fact, the dimensionless region depends on the pattern scale [22–24]. When $\lg \Lambda$ is smaller than 0.21, the shape of the dispersed particle would be strongly affected by the distinguish ability of the binarized image. When $\lg \Lambda$ is bigger than 0.72, the probability density, $P(\Lambda)$, is relatively smaller. Thus, the scanning density has a large effect on the result in this region. Furthermore, it can be concluded that different patterns may have different dimensionless regions due to the variation of the scale. However, the fractal dimensions of the patterns should not be affected by the dimensionless regions because they are only determined by the morphology of the dispersion phase. The inset of Fig. 12 is

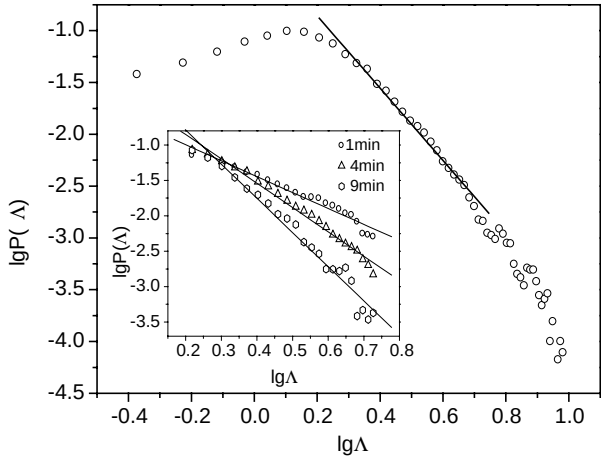

Fig. 12. Plot of lg $P(\Lambda)$ against lg Λ for PP/PA1010/PP-*g*-MAH (90/10/5) blends at 4 min during melt mixing. The inset is the part results of the linear regression in the dimensionless region during melt mixing.

the part results of the linear regression in the dimensionless region during melt mixing.

Fig. 13 shows that, with the increasing fraction of PP, there are two wave peaks and one valley in the curve. The increase of the dispersed phase fraction leads to the bigger fractal dimension. However, at the same time, the dispersion degree of the dispersed phase will becomes lower with the increasing dispersed phase fraction, which favors smaller fractal dimension. So, the increase in the dispersed phase fraction has two opposite effects on the fractal dimension. When the dispersed phase fraction is minor, the factor of the dispersed phase fraction is dominant. However, the dispersion degree is the dominant factor near the phase inversion. Thus, there are two wave peaks when the effects of these two factors approximate to be balance. Accordingly, there is a valley near the phase inversion. The figure also indicates that the fractal dimensions are bigger when PA1010 is the dispersed phase, demonstrating that PA1010 is more inclined to be dispersed phase. After feeding the compatibilizer, the fractal

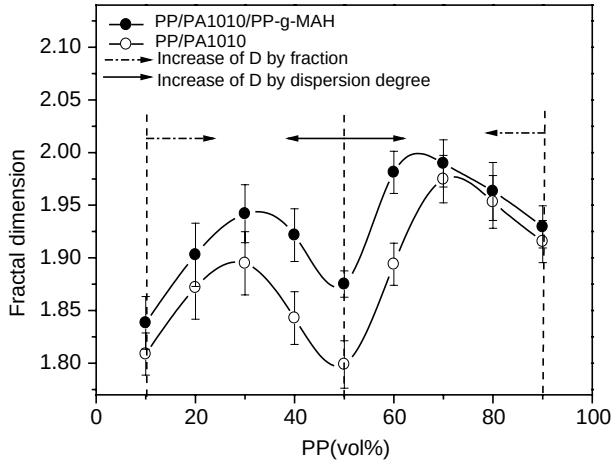

Fig. 13. Plots of *D* against the composition fraction for PP/PA1010/PP-*g*-MAH and PP/PA1010 blends.

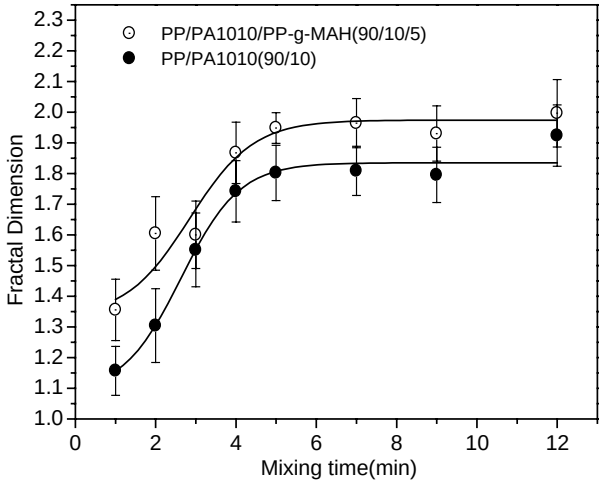

Fig. 14. Plots of *D* against the melt mixing time for PP/PA1010/PP-*g*-MAH and PP/PA1010 blends.

dimension become bigger, demonstrating that the dispersion degree becomes higher.

Fig. 14 reflects the temporal evolution of *D* in the PP/PA1010 blends before and after adding the compatibilizer during melt mixing. The figure shows that the fractal dimension is small but changes sharply at the initial stage (0–2 min). However, it falls on a master curve after 3 min and is almost unchangeable. The changes of the fractal dimension correspond to those of DP_{AV}, Λ and Λm. The increase of the fractal dimension indicates that the dispersion degree of the dispersed phase becomes higher because the fraction of dispersed phase is the same during melt mixing. From above analysis, it is clear that the fractal dimension, *D*, is an effective parameter to characterize the dynamics of the phase dispersion during melt mixing.

4. Conclusion

In general, the phase structure of the PP/PA1010 blends, before and after adding the compatibilizer, mainly form at the initial stage (0–2 min). It can be found that the distribution of the dispersed phase size is log–normal distribution. The parameters of the distribution, σ and e^{μ}, are two effective parameters to characterize the dynamics of phase dispersion. The results demonstrate that the structure of the dispersed phase during melt mixing evolves with dynamical self-similarity through the competition of break-up and coalescence of dispersed phase. Furthermore, a fractal dimension, based on the probability density of the character length, is introduced in this study. It can be seen that the fractal dimension is an effective parameter to characterize the dynamics of the phase dispersion during melt mixing. Two opposite factors, i.e. the fraction of dispersed phase and the dispersion degree, determine the change of the fractal dimension.

Acknowledgements

This work was supported by the National Nature Science Foundation of China. (Grant NO. 50390090). An

acknowledgment is due to Professor Lee Zhi-chong for his valuable suggestions.

Appendix A. Figure-estimation theory of log–normal distribution

In the present work, the figure-estimation theory [29] is introduced to judge whether the distribution of a variable is the log normal distribution.

If the logarithm in the log normal distribution is a common logarithm, the distribution function can be defined as

$$F(t) = \frac{\lg e}{\sqrt{2\pi}\sigma t} \int_{-\infty}^{t} \exp\left[-\frac{1}{2}\left(\frac{\lg t-\mu}{\sigma}\right)\right]^2 \mathrm{d}t, \quad t>0 \tag{A1}$$

Here, σ and μ are the standard deviation and number average of the distribution in $\ln(t)$, respectively. The distribution function is a monotonic ascending curve in the $t-F(t)$ coordinate system. It can be transformed into the expression of the standard normal distribution as follow

$$F(t) = \int_{-\infty}^{(\lg t-\mu)/\sigma} \frac{1}{\sqrt{2\pi}} \mathrm{e}^{-x^2/2}\mathrm{d}x = \Phi\left(\frac{\lg t-\mu}{\sigma}\right), \quad t>0 \tag{A2}$$

Because the standard normal distribution function, $\Phi(X)$, is strictly monotonic ascending, its inverse function exists. The inverse function can be defined as

$$\Phi^{-1}[F(t)] = \frac{\lg t-\mu}{\sigma} \tag{A3}$$

If let $Y=\Phi^{-1}[F(t)]$ and $X=\ln t$, the inverse function turns to be

$$Y = \frac{1}{\sigma}X - \frac{\mu}{\sigma} \tag{A4}$$

This is a linear equation in the $X-Y$ coordinate system. Its slope, which is positive, is $1/\sigma$. Its interception is μ/σ. Thus, a log normal distribution curve corresponds to an ascending line in the $X-Y$ coordinate system. Correspondingly, an ascending line in the $X-Y$ coordinate system will ascertain a log normal distribution function. It is clear that the an one by one relation between the ascending line in the $X-Y$ coordinate system and the log normal distribution function can be established.

Appendix B. The fractal dimension *D*

Let $F(t)$ be the distribution function. This distribution is related to the probability density $P(t)$ by

$$F(t) = \int_{t}^{+\infty} P(s)\mathrm{d}s \tag{B1}$$

If $F(t)$ is fractal, it is dimensionless. Thus, when the scale t is transformed to λt, the distribution of t requires the invariance

$$F(t) \propto F(\lambda t) \tag{B2}$$

for any positive λ. The only functional form that satisfies Eq. (B2) is the power law:

$$F(t) \propto t^{-D} \tag{B3}$$

where D is the fractal dimension [22–24]. The differential equation of Eq. (B3) is

$$P(t) \propto t^{-D-1} \tag{B4}$$

The logarithmic calculation can be done for both sides of Eq. (B4)

$$\lg P(t) \propto (-D-1)\lg t \tag{B5}$$

Eq. (B5) is the equation for calculating D by probability density $P(t)$.

References

[1] Paul DR, Newman S. Polymer blends, vols. 1 and 2. New York: Academic; 1976.
[2] Xanthos M. Reactive extrusion. Munich: Brown SB Inc.; 1992.
[3] Wang Y, Zhang Q, Fu Q. Macromol Rapid Commun 2003;24:231–5.
[4] Kawasumi M, Hasegawa N, Kato M, Usuki A, Okada A. Macromolecules 1997;30:6333–8.
[5] Galgali G, Ramesh C, Lele A. Macromolecules 2001;34:852–8.
[6] Wang H, Zeng CC, Elkovvitch M, Lee JK, Koelling KW. Polym Eng Sci 2001;41:2036–46.
[7] Kayano Y, Keskkula H, Paul DR. Polymer 1997;38:1885–902.
[8] Corté L, Beaume F, Leibler L. Polymer 2005;46:2748–57.
[9] Corté L, Leibler L. Polymer 2005;46:6360–8.
[10] Hashimoto T, Takenaks M, Lzumitani T. J Chem Phys 1992;97:679–89.
[11] Yuan XB, Sheng J, Lee XZ, Lee JS, Cai ZJ. Acta Polym Sin 2001;2:219–23.
[12] Scott CE, Macosko CW. Polymer 1995;36:461–70.
[13] Martin P, Maquet C, Legras R, Bailly C, Leemans L, van Gurp M, et al. Polymer 2004;45:3271–84.
[14] Burch HE, Scott CE. Polymer 2001;42:7313–25.
[15] Jana SC, Sau M. Polymer 2004;45:1665–78.
[16] Yang Y, Qiu F, Zhang H, Zhang J. Prog Nat Sci (Chin) 1998;8:513–22.
[17] de Gennes P. Scaling concepts in polymer physics. Ithaca, New York: Cornell University Press; 1979.
[18] Wang W, Shiwaku T, Hashimoto T. Macromolecules 2003;36:8088–96.
[19] Nakai A, Wang W, Hashimoto T. Macromolecules 1996;29:5288–96.
[20] Schmidt G, Nakatani AI, Butler PD, Karim A, Han CC. Macromolecules 2000;33:7219–22.
[21] Nakai A, Shiwaku T, Wang W, Hashimoto T. Macromolecules 1996;29:5990–6001.
[22] Takayasu H. Fractals in the physical sciences. Manchester: Manchester University Press; 1989.
[23] Mandelbrot BB. Fractal geometry of nature. New York: Freeman; 1983.
[24] Zhang JZ. Fractal. Beijing: Tsinghua University Press; 1995.
[25] Lee JK, Han CD. Polymer 2000;41:1799–815.
[26] Elemans PHM, Bos HL, Janssen JMH, Meijer HEH. Chem Eng Sci 1993;48:267–76.
[27] Limpert E, Stahel WA, Abbt M. Biosciences 2001;51:341–52.
[28] Wu S. Polymer 1985;26:1855–63.
[29] Fang KT, Xu JL. Statistics distribution. Beijing: Science Press; 1987.